

RESEARCH

Open Access



Evaluation of internal fixation stability of distal humerus C-type fractures based on musculoskeletal dynamics: finite element analysis under dynamic loading

Zhengfeng Jia^{1,2,3†}, Cheng Xu^{1,2†}, Weilu Gao^{1,2,3†}, Changsen Yang^{1,2,3}, Peifu Tang^{1,2*} and Jiantao Li^{1,2*}

Abstract

Purpose This study establishes a quantitative anatomical-mechanical-clinical decision-making mapping relationship using the Digital Intelligence Orthopaedic Technology, systematically analyses the dynamic biomechanical characteristics of distal humerus fracture in the postoperative period, and establishes the quantitative correlation between optimal strategies of plate configuration and safety thresholds for joint activities, to provide the scientific basis for optimizing internal fixation schemes and quantifying postoperative rehabilitation strategies.

Methods Upper limb muscle modeling was carried out in AnyBody software, muscle force, and other data were exported for finite distance solving and dynamic mechanical conditions were exported as the database for dynamic loading. Coupling the musculoskeletal dynamics simulation with finite element calculation, the elbow flexion-extension angle-muscle force-inner fixation stress transfer chain was established by AnyBody-Abaqus joint modeling technique to quantify the dynamic thresholds of the interface fracture micromovement (IFM) under different activity angles. The effects of different plate configurations (parallel plate, posterior medial plate, posterior lateral plate) on fracture stability and early healing were analyzed.

Results In this study, we systematically evaluated the biomechanical pattern of internal fixation of distal humerus fracture as well as the postoperative safe activity window and elucidated the enhancement path of functional recovery of distal humerus fracture utilizing AnyBody musculoskeletal dynamics analysis. By means of AnyBody musculoskeletal dynamics analysis, the humerus stress migration path showed anatomical-dependent characteristics, with gradient transfer from the hawks' fossa to the distal lateral condyle in flexion. Parallel plates stabilized the IFM in the bone healing window (0.06–0.20 mm) at 0–80° of flexion, whereas vertical plates breached the critical threshold (0.48 mm) in the IFM at > 30° of flexion. This reveals the law of mechanical matching between plate configuration and

[†]Zhengfeng Jia, Cheng Xu and Weilu Gao contributed equally to this work.

*Correspondence:
Peifu Tang
pftang301@126.com
Jiantao Li
lijiantao618@163.com

Full list of author information is available at the end of the article



© The Author(s) 2025. **Open Access** This article is licensed under a Creative Commons Attribution-NonCommercial-NoDerivatives 4.0 International License, which permits any non-commercial use, sharing, distribution and reproduction in any medium or format, as long as you give appropriate credit to the original author(s) and the source, provide a link to the Creative Commons licence, and indicate if you modified the licensed material. You do not have permission under this licence to share adapted material derived from this article or parts of it. The images or other third party material in this article are included in the article's Creative Commons licence, unless indicated otherwise in a credit line to the material. If material is not included in the article's Creative Commons licence and your intended use is not permitted by statutory regulation or exceeds the permitted use, you will need to obtain permission directly from the copyright holder. To view a copy of this licence, visit <http://creativecommons.org/licenses/by-nc-nd/4.0/>.

rehabilitation. There was a clear angle-dependent relationship between flexion angle and inter-fracture gap fragment motion (IFM). The IFM values tended to increase with increasing flexion and extension angles. When using parallel plates, allowing 0–80° of elbow flexion ensures better conditions for fracture healing. When using vertical plates, especially posterior medial plates active elbow flexion should be limited to about 30°.

Conclusions In this study, we quantified the mechanical effect of muscle contraction force on the stability of internal fixation of distal humerus C-type fracture and revealed the biomechanical law in the postoperative period; we established a simulation model of dynamic and static loading and proposed a ‘safe activity window’ for postoperative exercise, which confirms the high stiffness of the parallel steel plate and the control of the angle of early active activity ($\leq 80^\circ$ of flexion). Flexion of more than 30° in the case of vertical plates leads to shear micromotion overruns (> 0.48 mm).

Keywords Distal humerus fracture, Internal fixation, Finite element analysis, Musculoskeletal dynamics, Biomechanics, Fracture healing, Elbow motion

Introduction

Distal humerus fractures (DHF) account for only 2–6% of humerus fractures [1–3], but their treatment has always been an important challenge in trauma orthopedics due to their complex anatomy (30% involving the articular surface). The postoperative complication rate of Open Reduction Internal Fixation (ORIF) is as high as 34% [4, 5], and studies have shown that about 70% of patients with postoperative complications of distal humerus fracture have elbow instability or limited movement, which greatly affects the patient’s quality of life and ability to work [6].

For distal humerus fractures, especially intra-articular fractures, despite the obvious advantages of ORIF in restoring the congruence and stability of the articular surfaces, the postoperative performance in terms of restoration of elbow mobility, joint stiffness rate, and fracture healing rate still needs to be further improved [7]. Although elbow joint replacement can restore joint function in the short term, the long-term complication rate is high and does not apply to all patients. Therefore, the optimal treatment plan should be selected in clinical practice by taking into account the patient’s age, fracture type, soft tissue conditions, and other factors [2, 8]. In recent years, with the widespread use of double plate fixation, it has become the preferred option for an increasing number of surgeons due to its excellent performance in improving fracture healing rates and reducing complications, with higher fracture healing rates and lower risk of complications compared to other approaches [9, 10]. Frechette [2] et al. conducted a study on the outcomes of intra-articular distal humerus fractures treated with parallel precontoured plates in the elderly population. Their findings underscored the significance of precise anatomical reduction and stable fixation in minimizing postoperative complications and improving functional recovery. Similarly, Zdero [4] et al. reviewed the biomechanical design optimization of distal humerus fracture plates, emphasizing the need for robust fixation strategies to

enhance fracture healing and reduce the risk of non-union. However, there is still a great deal of uncertainty in the choice of position and configuration of double plate fixation. One of the key conflicts is how to simultaneously achieve the mechanical rigidity required for precise reconstruction of the articular surface and the biological flexibility required for early functional activity. Although the dual-plate system (parallel vs. vertical) significantly improves fixation stability (healing rate increased by 28%) compared with the single-plate system, its configuration strategy is still limited to the operator’s experience and lacks a quantitative biomechanical decision-making framework [11].

Existing studies have shown that the difference in therapeutic efficacy of dual plates essentially stems from the spatiotemporal heterogeneity of the stress transfer mechanism, with parallel plates demonstrating ultrarigid characteristics in the early stages of healing (0–1 month) under their biaxial locking design (47% improvement in resistance to axial loading) [12]. However, this resulted in a stress-shielding effect that inhibited bone scab mineralization; in contrast, vertical steel plates promoted biological remodeling in the late healing period by dispersing stress transmission (22% increase in elastic modulus recovery). Anatomical studies have confirmed that parallel plates are prone to form stress concentration zones in the coronal plane (mainly occurring at the plate-intercondylar ridge interface), whereas vertical plates optimize shear distribution through multiplanar fixation (34% reduction in articular surface stress fluctuations [13]). However, traditional static finite element models are difficult to capture the dynamic remodeling process of the scab and lack realistic motion simulation of muscular interventions, resulting in a disconnection between *in vitro* experimental findings and clinical practice [13].

With the rise of smart orthopedics, 3D modeling, and finite element analysis techniques are gradually being applied in the field of orthopedics. Three-dimensional modeling technology can transform the imaging data of

the patient's fracture site into a digital model, providing a visual basis for the development of surgical plans. Finite element analysis (FEA) provides a scientific method to evaluate the fixation effect by simulating the stress distribution of the fracture site under different internal fixation methods [14, 15]. It is pointed out that the finite element analysis technique can not only simulate the mechanical changes in the process of fracture healing but also analyze the influence of plate position, angle, and other parameters on fracture healing, which provides an important reference for optimizing the surgical plan. Despite the excellent performance of 3D modeling and finite element analysis techniques in orthopedic surgical planning, there are still some limitations in the application of these techniques [4]. Firstly, the sample size of in vitro mechanical studies is small and the conditions are demanding, making it difficult to truly reflect the mechanical properties in the in vivo environment [16]. Second, current studies mainly focus on the assessment of stiffness and stability of fixation modalities and lack dynamic analyses of postoperative rehabilitation and exercise environments. In addition, the lack of consideration of soft tissue conditions leads to some discrepancies between research results and clinical practice.

Intelligent orthopedic technology (finite element simulation, musculoskeletal dynamics) opens up a new path to crack the above problems, and the musculoskeletal dynamics simulation technology can analyze in detail the stress distribution, muscle force and joint force during joint activities by simulating the mechanical properties of muscles, bones, ligaments and other tissues in different movement states [17]. Currently, parametric bone scab growth algorithms have been able to simulate the mechanical evolution throughout the healing process (error < 8%), and the AnyBody-ANSYS coupled joint modeling technique has been innovated to achieve real-time analysis of muscle-driven internal fixation-bone

interface micromotion (IFM). The overall objective of this part of the study is to assess the effect of elbow flexion and extension on the mechanical microenvironment at the distal humeral fracture site. The aim was to assess the effects of elbow flexion and extension in the early healing process of distal humerus fractures through a combination of musculoskeletal dynamics and finite element analysis (FEM) to overcome these limitations and to provide more comprehensive data to support the clinic.

Method

Subjects of the study

After obtaining ethical approval from our hospital, the data of one healthy adult male with a neutral CT scan of the upper limb was acquired from the Digital Imaging and Communications in Medicine (DICOM) system of the hospital and burned on a CD-ROM in DICOM format.

3D modeling process of distal humerus fracture and internal fixation

After Mimics segmentation, the distal humerus was saved in STP format. The model was then imported into Solid Works 2022 and the cortical bone and cancellous bone were assembled through the origin fit command and saved in part format. Fracture surfaces were simulated according to the literature (open the model of the distal humerus, simulate the cutting plane, and simulate the fracture line from the lower edge of the ulnar falx fossa to the distal end, and in this part, we mainly modeled the AO/C-type fracture model (Fig. 1).

Parallel and vertical plate configurations were used in this study, and further distinction was made between posteromedial (Posteromedial, PML) and posterolateral (Posterolateral, MPL) versions of the vertical plate configuration. The construction of these models is based on the Finite Element Method (FEM) and model validation

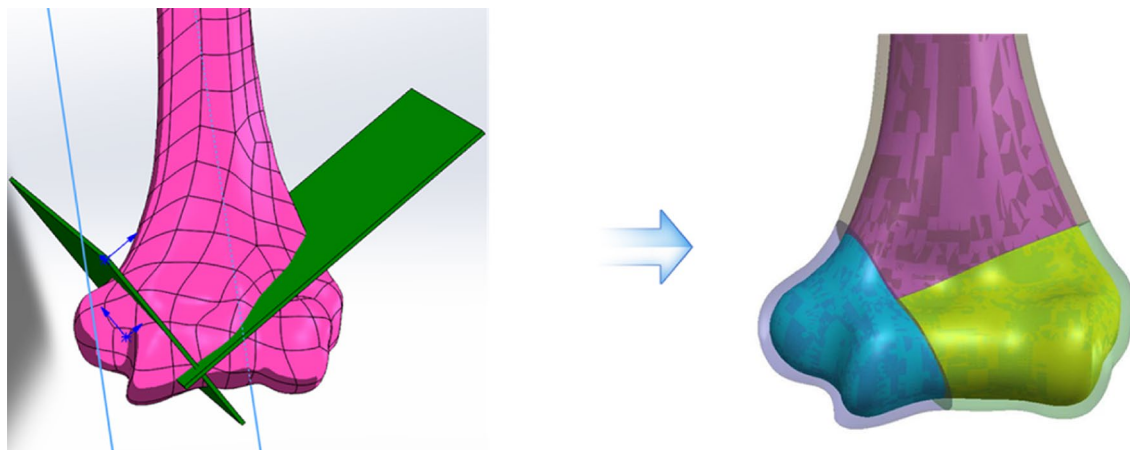


Fig. 1 SolidWorks distal humerus fracture model construction

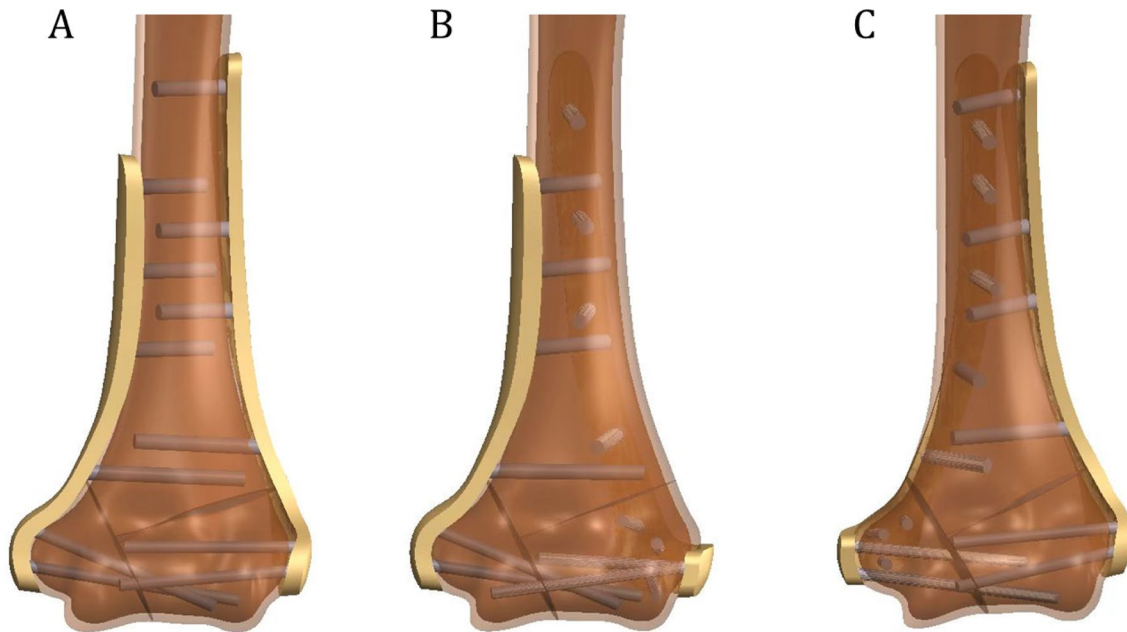


Fig. 2 3D modeling of three double plate placement positions; **A:** parallel 180° PL; **B:** vertical 90° posterolateral; **C:** vertical 90° posterolateral

Table 1 Properties of fixed model materials

Materials	Modulus of elasticity (MPa)	Poisson's ratio
Plates and screws	190,000	0.27
Cortical bone	17,000	0.33
Cancellous bone	5000	0.33

Table 2 Surface mesh parameters

Parameter	Maximum	Minimum
Bone	3 mm	0.5 mm
Plate	1.5 mm	0.5 mm
Screw	0.8 mm	0.3 mm

is carried out based on experimental results. The steps were as follows: three spatial plate configurations were constructed: parallel, posteromedial, and posterolateral. The number and positioning of the screws connecting the plate to the bone were modeled according to their implantation in clinical practice. Screw placement was performed using the general rules for inserting screws according to the AO guidelines and the stability optimization principles proposed by O'Driscoll, which are mainly applicable to parallel plates. During the numerical analysis, the screws connecting the plate to the bone block were simplified to an unthreaded model. Screws in the humeral shaft region were set to be modeled as cylinders with a diameter of 2.75 mm and an external thread diameter of 3.5 mm. Screws in the distal humeral region were modeled as cylinders with a diameter of 2 mm (Fig. 2).

Internal fixation material assignment and meshing

Bone material properties were set according to data from the literature [15], including modulus of elasticity and Poisson's ratio for cortical and cancellous bone. Material properties of steel plates and screws were also set according to data provided by the manufacturer (Tables 1 and 2). The material properties of the fracture surface and bone tissue were derived from the above validated literature. The bone cortical model was transversely isotropic, and the fracture interface friction coefficient was set to 0.4 based on experimental validation by Kruszewski [15] et al. These parameters have been shown to accurately simulate load transfer in distal humerus fracture models.

To ensure the reliability of our finite element analysis, we conducted a mesh convergence study. The percentage change in stress and displacement with mesh refinement was quantitatively assessed. The results showed that the maximum principal stress and displacement values changed by less than 5% with further mesh refinement, indicating that our results are independent of mesh density. This ensures the reliability of our finite element analysis.

Anybody model modeling process

(1) Source of base model: A 3D musculoskeletal model of the upper limb of a personalized individual was created using the AnyBody modeling system (AnyBody Technology, Germany), which is used for simulation and analysis of the musculoskeletal system. The standard musculoskeletal model of the upper limb (TLEM 2.0), which comes with AnyBody, was used, containing the anatomical parameters (starting and ending points,

physiological cross-sectional area, and length of the force arm) of 51 muscles. The 'Free Posture' model in the model library was selected, the muscles and bones unrelated to the experiment were deleted through code editing and execution, and the local coordinate system of the humeral head center was re-established in the model.

(2) Humerus model scaling: Bone-muscle scaling was implemented based on the subject's biometric parameters (body mass, height, and bony landmark geometry data). In this study, a validated homogenized scaling method was used to achieve anatomical fit by implementing simultaneous adjustments to bone mass attributes (inertial parameters) and topological nodes (joint centers, muscle attachment points). The scaling coefficient matrix was defined as a diagonal equiproportional form (Eq. 1). Geometric form and mechanical strength matching were accomplished simultaneously.

$$S = \begin{bmatrix} kl & 0 & 0 \\ 0 & kl & 0 \\ 0 & 0 & kl \end{bmatrix}, F = F_0 K_m^{\frac{2}{3}} \quad (1)$$

(3) Humerus muscle recruitment and inverse dynamics setup: Based on the principle of inverse dynamics, a multi-objective optimization algorithm was used to solve the muscle force distribution redundancy problem. The extreme value optimization method (Minimax strategy) was chosen for the muscle recruitment strategy, and the computational process satisfied the kinetic equilibrium constraints. The optimization method was pre-validated to be consistent with the polynomial optimization strategy in terms of muscle force prediction results (error < 5%).

To enhance the credibility of the muscle forces derived from the AnyBody model, we referenced EMG (Electromyography) studies. Specifically, Lai [18] et al. conducted a study validating the muscle forces in the upper limb using a similar musculoskeletal model. Their findings demonstrated that the muscle forces predicted by the AnyBody model are consistent with those measured by EMG, providing strong validation for our simulation results.

Coordinate matching between anybody and 3D reconstruction model based on the ICP algorithm

To achieve accurate mapping between musculoskeletal dynamics loads and finite element models, a cross-platform coordinate system transformation mechanism is required. Based on the humeral load data generated by AnyBody 8.0, this study achieves spatial data alignment through anatomical coordinate system calibration. Firstly, a local coordinate system with the center of rotation of the humeral head as the origin and extending along the long axis of the humeral stem was defined

in the AnyBody environment, which was associated with the geometric reference frame of the finite element model through the rigid body transformation matrix. The alignment was implemented using the reverse engineering toolset of Geomagic Studio 2022, and an iterative nearest-point algorithm was used to optimize the spatial match to ensure that the spatial error of anatomical landmarks between the dual platforms was less than 1.2 mm (root-mean-square value). This process is synchronized with the fine-tuning of the model scaling, and the effect of individual anatomical variability is compensated by dynamically adjusting the scaling factor ($kl \in 0.98-1.02$), which ultimately achieves an unbiased conversion of muscle force vectors and joint reaction forces to the finite element boundary conditions. The ICP algorithm (2, 3) was adopted to adjust the error values (Fig. 16), and finally, the two humerus models and the fracture model were perfectly matched (Fig. 3).

$$R^* = \operatorname{argmin}_R \frac{1}{2} \sum_{i=1}^n \|q_i - Rq'_i\| \quad (2)$$

$$t^* = p - Rp' \quad (3)$$

AnyBody load condition extraction

In the AnyBody scenario, internal strains are determined by multi-body simulation and numerical computation, and displacements are calculated based on known kinematics and inverse dynamics analysis of external forces. In joints which are usually treated as frictionless constraints and represented as segments, a specific number of degrees of freedom are limited depending on the type of segment. Between each segment, forces from joint contact, muscles, gravity, inertia, and external loads act through integration. Dynamic motion is captured by AnyBody, enabling realistic estimation and reliable computational results.

With the AnyFE2Abq interface module integrated with AnyBody platform, this study realizes the spatial mapping of finite element model coupled with a biomechanical environment. The elbow flexion-extension kinematic driving logic is configured through parametric scripts to establish the inverse dynamics computational framework. The kinematic simulation covers the complete flexion-extension cycle (flexion phase: $10^\circ \rightarrow 130^\circ$, extension phase: $130^\circ \rightarrow 10^\circ$), and the joint contact dynamics response is obtained by iterative solving (Fig. 4). At this point, the boundaries of muscle forces, joint forces, and load torques are defined by the inverse kinetics, which are manually registered by Geomagic Studio in *.iges and exported as *.inp.

Based on the above settings, the execution language was edited to simulate the inverse dynamics of the elbow

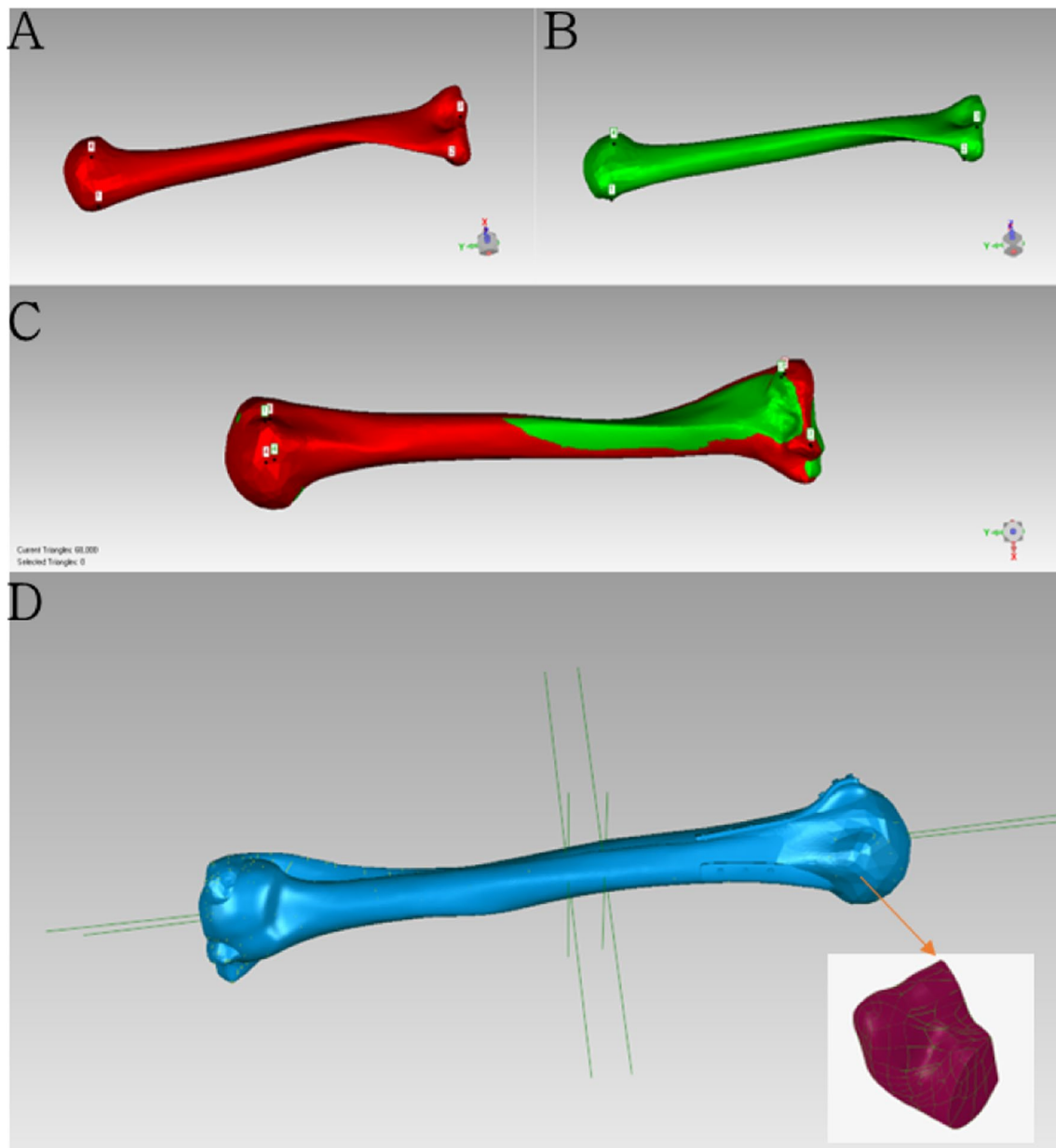


Fig. 3 Reconstructed humerus model with AnyBody model coordinate matching. **A:** AnyBody humerus model; **B:** 3D reconstructed humerus model; **C:** Coordinate matching; **D:** Detail of fracture surface matching

flexion analysis. The humerus model was exported and the derived joint reaction forces, muscle forces, and moments were applied to the distal humerus fracture using the registration feature of Geomagic Studio and the 'AnyFE2Abq' option of the AnyBody plug-in. The muscle attachment/articulation point is partially coupled to the adjacent humeral surface (Fig. 4). The boundary conditions and the distal humerus fracture plate system model were then imported into Abaqus 20.0 (Dassault Aviation, USA) and the bone was modeled as a linear, elastic, and isotropic material. Cortical and cancellous bone geometries were globally meshed using tetrahedral

cells, and plates and screws were meshed using hexahedral cells. It was assumed that all interfaces between bone, screws, and steel plates were bonded. The contact between the fracture lines was set to be friction, and the finite element model of the fracture-plate system was subjected to a standard mesh convergence analysis, where the key parameters were almost independent of the mesh size plate deformation and intersegmental displacement varied by less than 5%, and were also not significantly affected by the mesh density. The element sizes of the humerus, plate, and screw were 3 mm, 1.5 mm, and 0.8 mm, respectively, and the numbers of elements

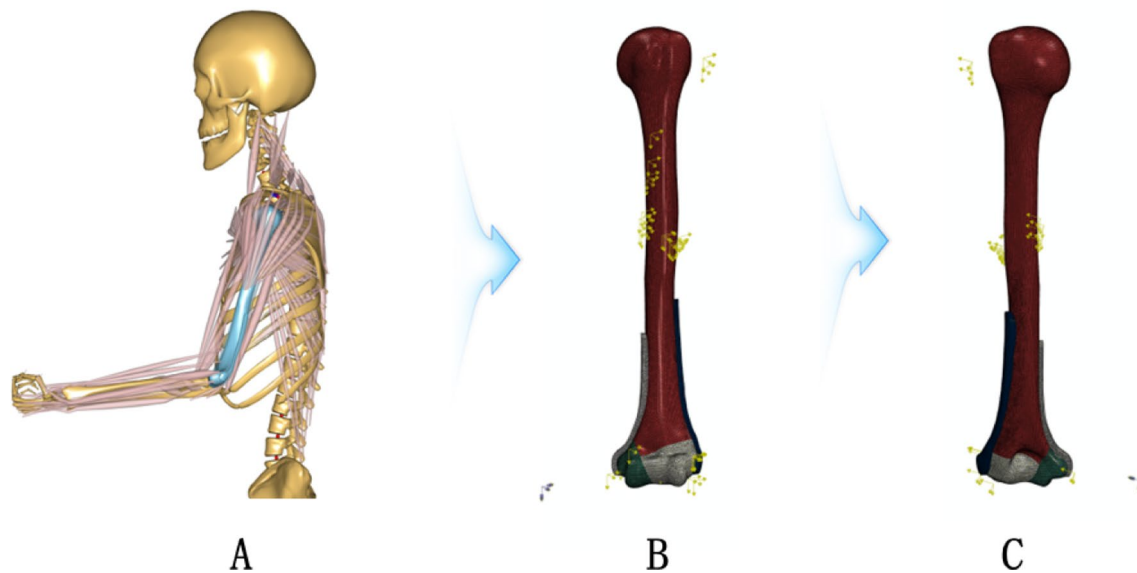


Fig. 4 Dynamic loading and boundary conditions. **A** An Individualised muscle model; **B** anterior view of the humeral loading section; **C** posterior view of the humeral loading section

and nodes in the finite element model were 288,400 and 64,686 for the humerus, 14,500, and 19,164 for the plate, and 8640 and 10,283 for the screw, respectively.

Data reliability analysis and validation based on the anybody model

In this study, the reliability of the AnyBody musculoskeletal model was systematically evaluated for daily loading analysis of the humerus through anatomical shape modeling and a biomechanical plausibility validation system. First, the geometric validation based on statistical shape modeling (SSM) showed that the alignment error of key anatomical marker points was controlled within 1.2 mm. Particularly, in the modeling of mechanical conduction paths in complex curved regions of the distal humerus (e.g., hawks' fossa, talonavicular groove), it provided an accurate morphological benchmark for personalized splint design. At the kinetic level, the biomechanical rationality of the muscle conduction model was corroborated. Yong et al. [19] verified the theory of load reduction of upper and lower limb muscles associated with wearing an exoskeleton based on the muscle kinetic analysis and the AnyBody modeling system and verified the reliability of the AnyBody muscle data through experimental data. The disadvantage of EMG is that it can only measure the muscles close to the surface of the skin. In contrast, AMS performs normalization by exporting the maximum muscle activity values for each muscle group through the AnyBody Managed Model Repository (AMMR), which is a procedure based on virtual template information provided by anthropometry. Halonen [20] et al. built and validated a 3D model of the humerus through the AnyBody model, which is in agreement with

our muscle force extraction results. Unlike previous literature validation methods, we performed geometric validation through the statistical shape model built in Chap. 1 to ensure model matching.

Abaqus finite element analysis solutions

The above *.inp file was imported into Abaqus (Fig. 5) and torque loading and position adjustment were performed manually according to the anatomical attachments. Ten-time points (one segment every 13°) were set for normal humerus and 13-time points (one segment every 10°) were taken for internal fixation. Each segment corresponded to a time point in the elbow flexion motion of the AnyBody software and was solved by finite element analysis.

Extraction of the main results of musculoskeletal dynamics

Stress and displacement analysis

Assess the equivalent stress distribution of the bone tissue based on the Von Mises stress cloud; extract the maximum principal stress distribution, analyse the dynamic evolution characteristics of the stress concentration area under different angles, and draw the maximum stress transfer map. Quantify the humeral commissure displacement and X/Y/Z direction displacement components; analyze according to the total displacement.

IFM analysis of distal humerus fracture block

The IFM extraction methods include the region of interest (ROI) calculation method as well as the automated extraction of node displacements by APDL commands, the latter of which is adopted in this part of the study after extensive pre-experimental labeling, where the

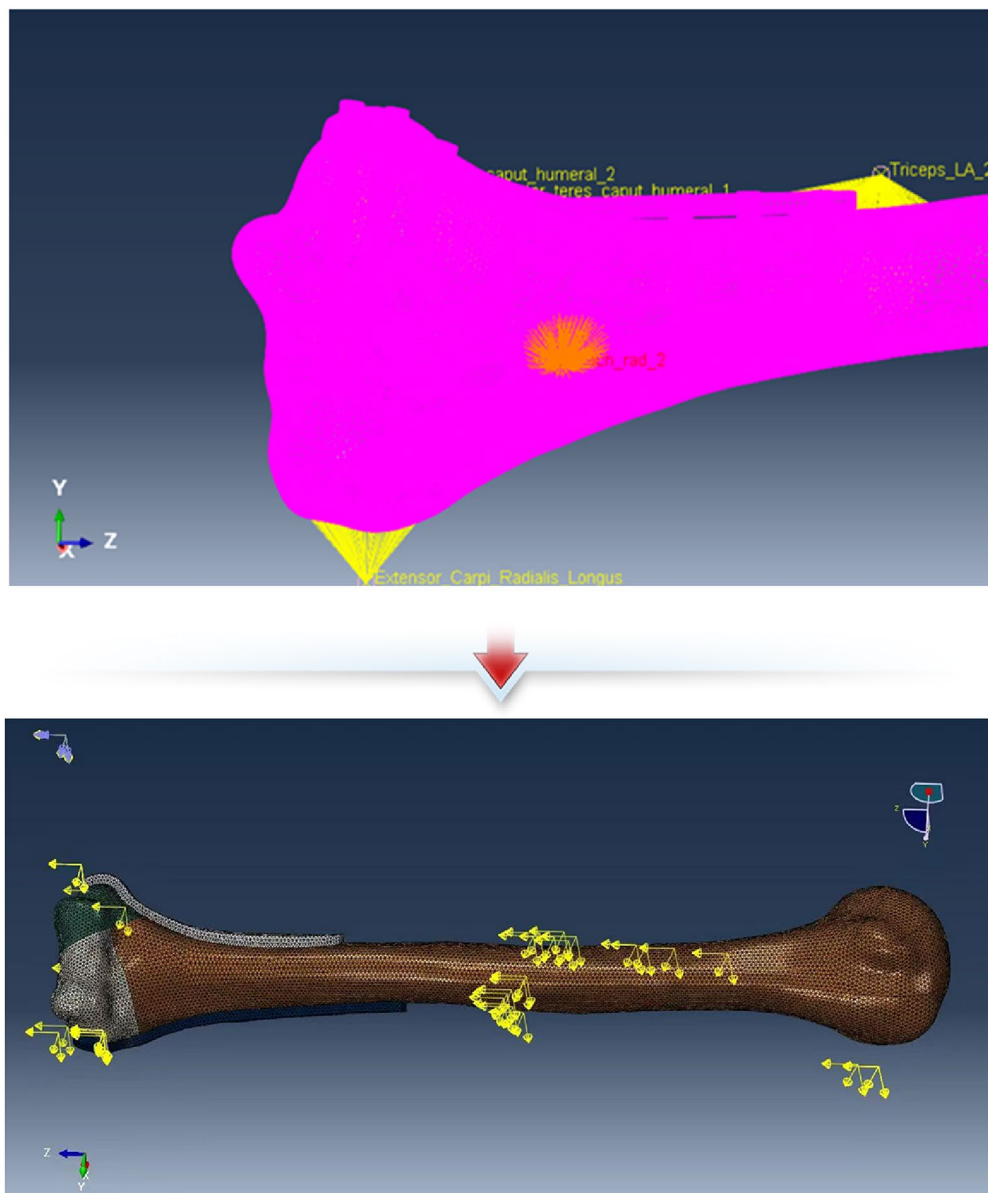


Fig. 5 Mechanical loading and solution process of Abaqus FEA

fracture blocks are usually defined as different geometrical portions or sets of nodes in the finite element model. We ensure that each fracture block has a separate set of nodes in the model. Subsequently, node displacement extraction was carried out, where the node displacement data for each fracture block was extracted after the Abaqus solution was completed, and the displacement values of the nodes (X, Y, and Z directions) were derived. The relative displacement between two nodes can be calculated directly using the 'Relative Displacement' option in Abaqus, and the final result is expressed as the total displacement. Intra-articular fractures are more demanding in terms of IFM, which usually needs to be kept below 0.2 mm to ensure accurate repositioning of the articular

surfaces and cartilage repair [21]. The risk of non-union or traumatic arthritis of intra-articular fractures is significantly increased when the IFM exceeds 1 mm. Steiner's Tangential Stiffness Threshold Theory: the clinical risk of IFM increases dramatically with tangential stiffness < 300 N/mm [21].

Von mises maximum stress results

The Von Mises stress solution is implemented by driving a finite element model through AnyBody musculoskeletal dynamics data (muscle force/joint torque), which maps the dynamic muscle loads to Abaqus quasi-static boundary conditions; after the solution, the peak mechanical state at each flexion angle is extracted as a loading source;

Table 3 Von mises stress values (MPa) for different flexural angles

Flexion angle	1	2	3	4	5	6	7	8	9	10
Flexion 0°-130°	10.43	7.02	5.02	4.61	4.59	4.46	4.21	3.92	3.87	3.87
Extension 130°-0°	7.80	7.80	8.49	9.80	10.1	9.60	8.71	8.06	7.88	7.88

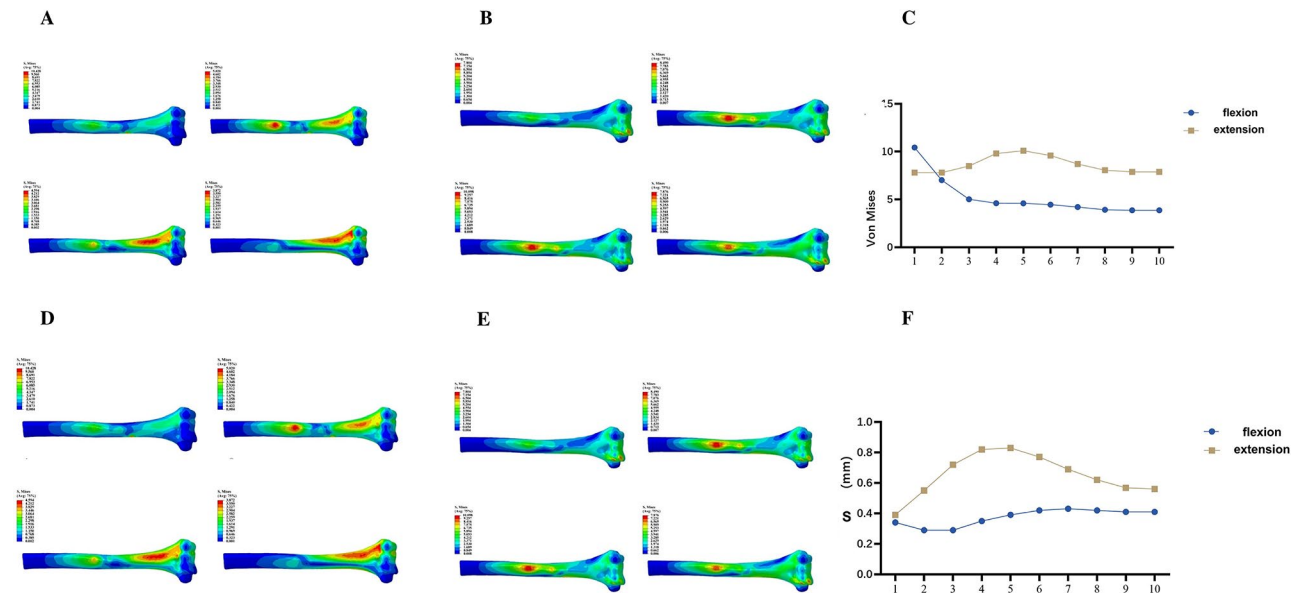


Fig. 6 **A** Dynamic change process of the maximum principal stress area during flexion; **B** Dynamic change process of the maximum principal stress area during extension; **C** Dynamic change pattern of the maximum principal stress area during elbow flexion and extension. In flexion from 0°-130°, the maximum principal stress decreases with the increase of the angle, and in extension, the maximum principal stress increases and then decreases with the increase of the angle, and reaches the peak at about 80°; **D-F** the relative displacement rule of the humerus in different flexion and extension angles. In flexion from 0°-130°, the relative displacement decreases and then increases with the angle and reaches the peak at about 40°. In extension, the relative displacement increases and then decreases with increasing angle, reaching a peak at about 80°

and a multi-angle batch computation is subsequently executed to locate the maximum stress hotspot of the steel plate system. The coupled method maintains the real muscle force time-series characteristics (AnyBody data accuracy $\pm 7\%$) and efficiently assesses the failure risk of the endoprosthesis over the full kinematic cycle.

Result

Von mises stress maps of the humerus at different flexion and extension angles, changes in the relative displacement of the humerus at different flexion and extension angles, and the migration path of the maximum principal stress zone

In flexion from 0°-130°, the maximal principal stress decreases with increasing angle, and in the migration path: the zone of maximal principal stress gradually migrates from above the Olecranon fossa (0°) along the lateral humerus to the lateral condyles (90–120°). During extension, the maximum principal stresses increased and then decreased with increasing angle, reaching a peak at approximately 80°. The dynamics of Von Mises stresses at different flexion and extension angles are reflected in Table 3, and their corresponding diagrams and maximum migration paths are shown in Figs. 6A and C and 7.

In flexion from 0°-130°, the relative displacement decreases and then increases with angle, peaking at about 40°. In extension, the relative displacement increased and then decreased with increasing angle, reaching a peak at about 80°. The dynamics of the relative displacement of the humerus at different flexion and extension angles is reflected in Table 4, and its corresponding graph is shown in Fig. 6D and F.

Effect of different flexion angles on inter-fragment interval fragment motion (IFM) in distal humeral fractures

Through finite element analysis, we extracted the inter-fragment displacement (IFM) values at different flexion angles (Table 5; Fig. 7). The results showed that the elbow flexion angle had a significant effect on the IFM values. At high flexion angles (>90°), the IFM values increased significantly, especially in the posterior-lateral plate configuration, where the IFM exceeded 0.5 mm, significantly increasing the risk of fracture non-union. In the parallel plate configuration, the IFM remained within the range of 0.01–0.20 mm from 0–80°, which is following the ‘optimal mechanical guidance theory’ (OPT) of bone healing. In conclusion, the use of parallel plates, which allow the elbow to be flexed from 0–80°, ensures better conditions

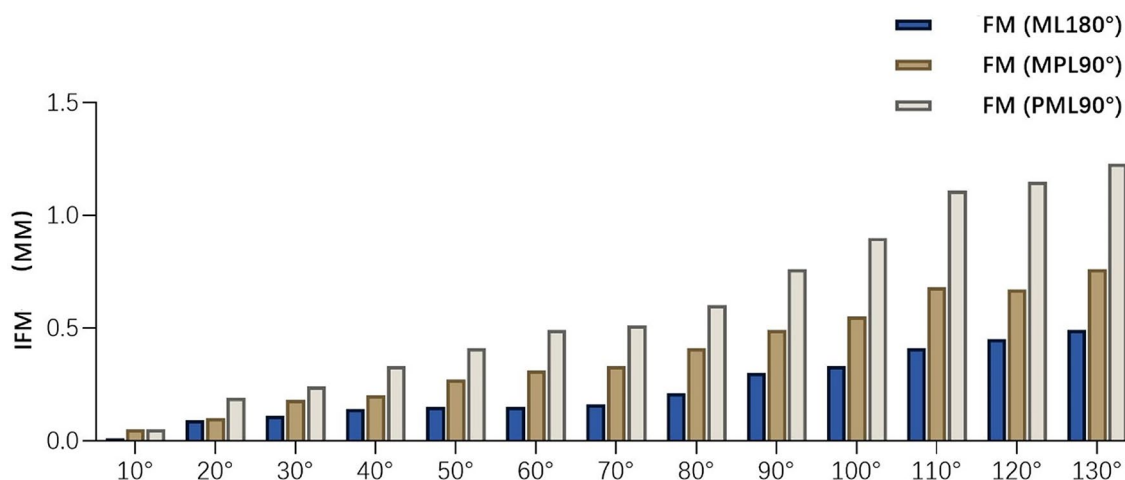


Fig. 7 IFM values of the distal humerus at different flexion angles (mm)

Table 4 Changes in relative humeral displacement at different flexion and extension angles (mm)

Time	1	2	3	4	5	6	7	8	9	10
Flexion 0°-130°	0.34	0.29	0.29	0.35	0.39	0.42	0.43	0.42	0.41	0.41
Extension 130°-0°	0.39	0.55	0.72	0.82	0.83	0.77	0.69	0.62	0.568	0.56

Table 5 IFM values of the distal humerus at different flexion angles (mm)

Agle of flexion (°)	Total IFM (PLL180°)	Total IFM (MPL90°)	Total IFM (PML90°)
10	0.01	0.05	0.05
20	0.09	0.1	0.19
30	0.11	0.18	0.24
40	0.14	0.20	0.33
50	0.15	0.27	0.41
60	0.15	0.31	0.49
70	0.16	0.33	0.51
80	0.20	0.41	0.60
90	0.30	0.49	0.76
100	0.33	0.55	0.90
110	0.41	0.68	1.11
120	0.45	0.67	1.15
130	0.49	0.76	1.23

PLL180°: Parallel 180°; MPL90°: Posterolateral 90°; PML90°: Posteromedial 90°

Table 6 Maximum von mises stress values at different buckling angles (MPa)

Agles(°)	Maximum stress Von Mises of flex-ion (PLL180°)	Maximum stress Von Mises of flex-ion (MPL90°)	Maximum stress Von Mises of flex-ion (PML90°)
10	156.780	303.725	141.549
20	158.758	307.003	143.133
30	161.835	311.966	145.619
40	166.681	319.513	149.579
50	163.511	310.265	146.253
60	196.008	283.198	132.377
70	169.191	239.645	113.527
80	141.393	196.733	94.436
90	118.104	161.583	78.590
100	98.436	133.105	65.351
110	81.865	110.459	54.314
120	67.838	92.611	45.091
130	55.670	78.405	37.300

PLL180°: Parallel 180°; MPL90°: Posterolateral 90°; PML90°: Posteromedial 90°

for fracture healing when parallel fixation is used. Worse conditions occur when vertical plates are used, especially posterior medial plates. In this case, active elbow flexion should be limited to about 30°.

Results of the effect of different flexion angles on the stress change of elbow joints

To assess the weakness of the fracture fixation, we analyzed the maximum Von Mises stress distribution for different plate configurations (Table 6). The results showed that the maximum Von Mises stress gradually increased

and then gradually decreased during elbow motion (Fig. 8).

Parallel steel plates (ML180°)

The peak value is 88.15±5.72 MPa (full angle range) and the maximum value occurs at 60° flexion position (196.008 MPa). The maximum stress values are higher for parallel steel plates at smaller buckling angles (10°-60°) and gradually decrease with increasing buckling angle. At 150°, the maximum Von Mises stress decreases to a minimum (22.120 MPa). The stresses are mainly concentrated

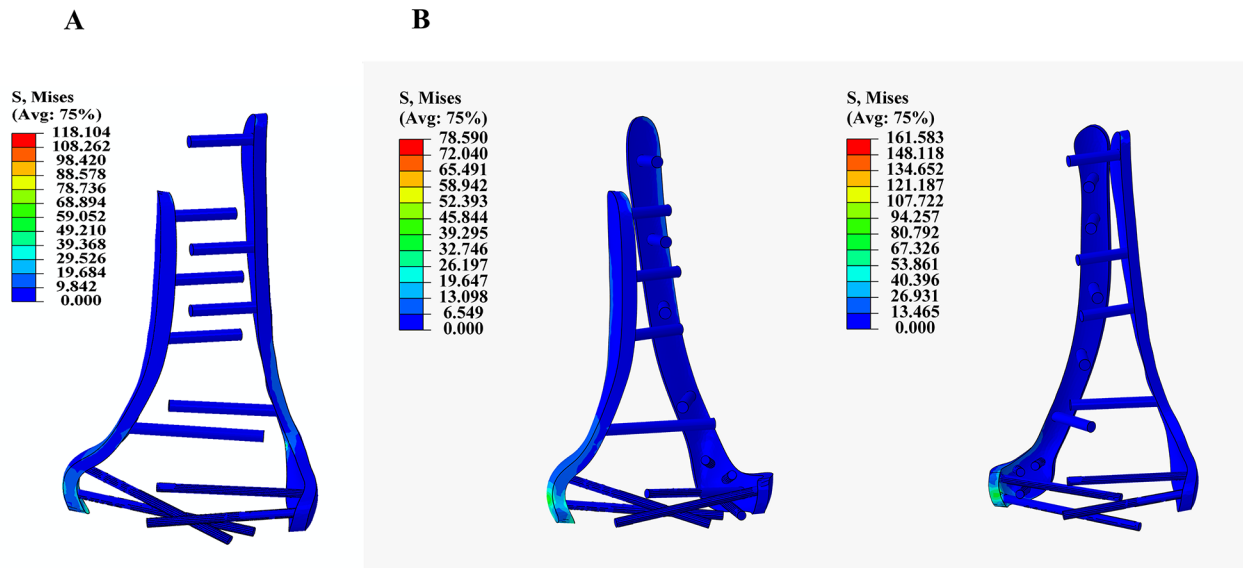


Fig. 8 Maximum von Mises stress values for different buckling angles

in the middle section of the steel plate, and the maximum principal stress is much lower than the yield strength of the titanium alloy (900 MPa), which indicates that it has good structural stability.

Posterolateral plate (MPL 90°)

The critical point of fixation failure of the posterior lateral vertical steel plate was 110° of flexion (298.91 MPa), and the stresses were concentrated on the medial surface of the fifth screw hole. The stress values were higher at smaller flexion angles (303.725 MPa at 10°) and decreased rapidly as the flexion angle was increased, and especially after 60°, the values of the stresses were significantly reduced. At 150°, the maximum Von Mises stress decreased to 42.375 MPa. The posterolateral plate showed a concentration of stress at the screw-bone interface with a maximum principal stress of 350 MPa, which may trigger micromotion and increase the risk of infection and non-healing.

Medial plate (PML 90°)

The stress values of the posterior medial plate decrease gradually with increasing flexion angle, with a steep increase in stress (0.32 MPa/°) in the first 20° of the flexion section, and then showing a more gentle trend. The maximum Von Mises stress is 141.549 MPa at 10° and decreases to 19.995 MPa at 150°. The stresses are relatively high at smaller buckling angles, but as the angle increases, the distribution of the stresses is gradually homogenized, which reduces the localized stress concentration.

Discussion

In this part of the study, musculoskeletal dynamics and finite element analysis methods were comprehensively applied to thoroughly investigate the biomechanical effects of elbow flexion and extension angles and plate configuration on the healing process of distal humerus fractures. The findings elucidated the biomechanical evolution of the distal humerus in the full range of elbow flexion and extension (0°-130°), as well as the anatomical dependence of the humeral stress migration path, with a gradient from the falciform fossa to the distal lateral condyle in flexion, coupled with the anatomical characteristics of the lateral condylar bone mineral density (1.12 g/cm³) and the medial cortical thickening of 22%. Revealing the nature of the lateral condyle as a mechanically weak zone, there was a clear angle-dependent relationship between flexion angle and inter-fracture interval fragment motion (IFM). The IFM values tended to increase with increasing flexion and extension angles, and secondly, there were significant differences in the biomechanical performance of different plate configurations on fracture stability. Parallel plates maintained high axial stiffness at all flexion angles, much higher than posterolateral plates. This high stiffness property allowed parallel plates to effectively control the IFM values and maintain them within a range favorable to bone healing.

We found that there is a dynamic transfer law of muscle load during elbow flexion, with the maximum principal stress increasing with increasing angle in flexion from 0°-130°, and our results are consistent with muscle forces previously reported in the literature, corroborating the idea that the brachialis muscle dominates the load in flexion [22]. Kong et al. performed a consistency validation of AnyBody’s loading data, confirming the reliability of

their data [19], and externally validated the muscle forces in the upper limb, which were consistent with our experimental results. In the maximum principal stress migration path: the maximum principal stress area migrated gradually from above the falciform fossa (0°) to the lateral condyle ($90\text{--}120^\circ$) along the lateral humerus. During extension, the maximum principal stresses first increased and then decreased with increasing angle, reaching a peak at approximately 80° . In the present study, we found that the stress in the lateral epicondyle increased significantly at 90° of flexion, and the gradient migration of the region of maximum principal stress along the lateral epicondyle ($0^\circ\rightarrow 120^\circ$) suggested a dynamic feedback mechanism of skeletal strain adaptation, which formed a mechanistic-structural coupling with the anatomical distribution of the bone density (mean density of the lateral epicondyle 1.12 g/cm^3 vs. 1.07 g/cm^3 of the trolley) [23]. The anatomical characterization of this region as a mechanically weak point was also verified [24]. Gerd et al. [25] measured the distribution of bone mineral density (BMD), trabecular BMD (BMD), and cortical thickness (CTh) of the distal humerus using peripheral quantitative computed tomography, and the CTh of the medial column in the supracondylar region was on average 22% higher in the medial column as compared to the lateral one, which also demonstrated the mechanically weak zone of the lateral condyle. In agreement with our findings, stress concentrations should be avoided during surgical fixation to ensure good functional recovery.

Boundary conditions are often simplified or ignored in most FEA studies [15], even though the humeral muscles play an important role in loading and constraint. Muscle and ligament interactions contribute significantly to motion. The setup of boundary conditions for our model ensured reliable results, despite the lack of cadaveric experimental validation. We dynamically map the muscle activation timings to the evolution of the fracture micro-environment in this section, breaking through the limitations of traditional static FEA load simplifications. The results show that elbow flexion angle has a significant effect on IFM values. In particular, at high flexion angles ($>90^\circ$), IFM values increased significantly, which may lead to poor fracture healing. In the posterolateral plate configuration, an IFM of more than 0.5 mm significantly increased the risk of fracture nonunion. In parallel plate configurations, the IFM remained within the range of 0.06–0.15 mm, which is following the ‘optimal mechanical guidance theory’ (OPT) of bone healing [21].

For C-type fractures of the distal humerus (intra-articular fractures), the surgical principle is strong fixation and allowing early movement, and with this requirement comes a relatively high complication rate [5], and we have used threshold analysis in this section to introduce a threshold of relative displacement of the fracture block

to establish a safe postoperative window of movement. When parallel plates are used, elbow flexion of $0\text{--}90^\circ$ is allowed, which ensures better fracture healing conditions when parallel fixation is used. Worse conditions occur when vertical plates are used, especially posterior medial plates. In this case, active elbow flexion should be limited to about 30° . This finding is structurally consistent with previous finite element analyses that the stability of the plate fixation system is significantly reduced at high angles of flexion, leading to an increase in the IFM value and an increased risk of fracture non-union [26]. By combining cadaveric experiments and finite element analysis, and also by analyzing the IFM values, Kruszewski [15] et al. concluded that no plate configuration ensured distal humerus fracture union when the elbow was allowed to be fully flexed while holding a 1 kg weight in the hand. The exercise program given was such that when parallel plates were used, flexion in the range of $0\text{--}90^\circ$ under load was acceptable. This is consistent with our findings.

Meanwhile, by comparing the maximum stress values of the three types of double plate fixation, we found that parallel plates maintained high stiffness at all flexion angles, ensuring that the axial component of the IFM was in the optimal range, which is following the ‘optimal mechanical guidance theory’ (OPT) of bone healing [21]. In contrast, the posterior lateral plate showed lower stiffness at high flexion angles, resulting in an IFM of more than 0.5 mm, which significantly increased the risk of non-healing. This result is consistent with the findings of Kruszewski [15] et al. who found that posterior lateral plates were less stable at high flexion angles, leading to poor fracture healing. In distal humerus fractures, early functional exercise or Continuous Passive Motion (CPM) [27, 28] is of great significance for the recovery of post-operative elbow flexion and extension, which requires absolute stillness of the internal fixation as well as strong intra-operative fixation, which is the principle of plate and screw fixation of the distal humerus.

As an emerging technological tool, musculoskeletal dynamics simulation has shown great potential in the field of orthopedics [29]. Traditionally, the study of fracture healing has relied on static finite element analysis, which provides some biomechanical information but has limitations in its ability to simulate the fracture healing process in complex physiological environments. Musculoskeletal dynamics simulation can reflect the biomechanical environment during fracture healing more realistically by combining the dynamic movements of muscles, bones, and joints, providing a new perspective for researchers and clinicians [30]. Traditional finite element analyses are usually based on static conditions, ignoring the effects of muscle contraction, joint motion, and other factors on fracture healing. By introducing dynamic motion, musculoskeletal dynamics simulation

can mimic real physiological environments and more accurately assess biomechanical changes at the fracture site [31, 32]. For example, in this study, by simulating the motion of the elbow joint under different flexion angles, we found that the flexion angle had a significant effect on the IFM value, which could not be observed under static conditions. Musculoskeletal dynamics simulation not only covers mechanical analysis but also combines knowledge from several disciplines such as biology, anatomy, and engineering [33]. This multidisciplinary integration enables a comprehensive assessment of the biomechanical conditions of fracture healing from multiple perspectives. This part of the study not only assessed the stiffness and stability of different plate configurations but also revealed the specific effects of different flexion angles on fracture healing through precise measurements of IFM.

This dynamic simulation of personalized elbow motion presented in this section provides loading conditions for finite element analysis and minimizes measurement errors in internal mechanics. In clinical work, musculoskeletal biomechanics tested by AnyBody can also be applied to joint replacement, implant design, and daily activities [34], as the results of this simulation experiment are consistent with clinical practice. Its reliability is demonstrated in Part II, and the computational model we have developed in this part of the study will identify a position where joint forces are minimized, thus potentially reducing pain and facilitating fracture healing. The clinical significance of our results is that minimizing joint forces from the onset of injury may prolong pain-free living. Myodynamic outputs can be verified experimentally, such as by electromyography or previous literature. For example, Dubovsky [35] et al. investigated the behavior of the shoulder joint in propelling a wheelchair and proposed a rigid body musculoskeletal model of the upper limb, suggesting a link between joint forces and pain. Ni et al. [36] investigated the direction of hand movement by implementing AnyBody, a tool based on an empirical statistical model that estimates forces at different points and in various directions, highlighting the biomechanical advantages due to the direction of the force application.

Although the present study provides comprehensive dynamic biomechanical data, there are some limitations. Firstly, this study was based on a model of a single healthy individual, and more diverse fracture types and bone status should be included in the future to improve the generalisability of the study. Modeling about osteoporosis has not been represented in this study, which is the work of the current team study. Second, long-term clinical follow-up data would help validate the accuracy of biomechanical predictions and provide more direct evidence support for plate selection and rehabilitation programs. In addition, exploring the micromotor wear

mechanism of the plate-bone interface under dynamic loading will help to further optimize internal fixation design and improve the success rate of fracture healing. In addition, the accuracy of biomechanical predictions needs to be verified in conjunction with clinical results to provide more precise guidance for clinical practice. We quantified the finite element loading conditions based on and musculoskeletal dynamics data in this study to improve the biomechanical patterns of different flexion and extension angles after internal fixation of the distal humerus, which provides biomechanical guidance for clinical rehabilitation. In the future, this part of the data should be used in prospective clinical trials in conjunction with patients' and physicians' rehabilitation programs, and the biomechanical data constructed with the angle of motion and internal fixation modalities should be applied in the clinic.

In summary, this part of the study comprehensively evaluated the effect of elbow flexion on the early healing of distal humerus fractures by introducing musculoskeletal dynamics simulation combined with dynamic finite element analysis. The results showed that the flexion angle had a significant effect on the IFM value, and different plate configurations also had significant differences in fracture stability. By choosing a reasonable plate configuration and strictly controlling the flexion angle, the fracture healing environment can be effectively improved and the risk of complications can be reduced. As an innovative technical means, the simulation of musculoskeletal dynamics provides a new perspective for the study of fracture healing, and it is expected to play a greater role in future research in combination with AI artificial intelligence.

Conclusion

In this part, the biomechanical evolution of the distal humerus in the full range of elbow flexion and extension (0° - 130°) was elucidated by musculoskeletal dynamics simulation, as well as the stress migration path of the humerus showed anatomically dependent characteristics, and the stress and IFM data of various double plate types were proved in combination with the finite element analysis, and the present study demonstrated that the fixation device stabilizes the double-column structure regardless of whether it was fixed in parallel or vertical fixation. The healing environment of distal humerus fractures can be effectively improved and the risk of complications can be reduced by rationally choosing plate configurations and strictly controlling the flexion angle. When parallel plates are used, allowing the elbow to be flexed by 0 – 80° can ensure better fracture healing conditions. When using vertical plates, especially posterior medial plates active elbow flexion should be limited to about 30° .

Supplementary Information

The online version contains supplementary material available at <https://doi.org/10.1186/s13018-025-05876-z>.

Supplementary Material 1

Acknowledgements

Not applicable.

Author contributions

Li JT, Tang PF and Xu C: Conceptualization; Tang PF: Study design, data collection and analysis; Jia ZF: Original manuscript writing; Gao WL, Jia ZF: Language check, review & editing. All authors commented on previous versions of the manuscript. All authors read and approved the final manuscript.

Funding

This study was supported by the special funding of the National Clinical Research Center for Orthopedics, Sports Medicine and Rehabilitation. We declare that no funds, grants, or other support were received during the preparation of this manuscript. This work was supported by the Data-driven research on the development and application of ulnar coronoid prostheses (22QNCZ045) and the Special Funding of the National Clinical Research Center for Orthopedics, Sports Medicine and Rehabilitation.

Data availability

No datasets were generated or analysed during the current study.

Declarations

Ethics approval and consent to participate

The study was approved by the Hospital Ethics Committee. Ethics number: 2024KY005-KS001, and all procedures followed the ethical standards of the institutional and/or national research councils, as well as the Declaration of Helsinki of 1964 and its later revisions or similar ethical standards in research involving human participants. Written informed consent was obtained from all participants in the study.

Consent for publication

Not applicable.

Competing interests

The authors declare no competing interests.

Author details

¹Senior Department of Orthopedics, The Fourth Medical Center of Chinese PLA General Hospital, Beijing 100048, China

²National Clinical Research Center for Orthopedics, Sports Medicine and Rehabilitation, Beijing, China

³Graduate School of Medical School of Chinese PLA Hospital, Beijing, China

Received: 16 March 2025 / Accepted: 30 April 2025

Published online: 17 May 2025

References

- Bergh C, et al. Fracture incidence in adults in relation to age and gender: A study of 27,169 fractures in the Swedish fracture register in a well-defined catchment area. *PLoS ONE*. 2020;15(12):e0244291.
- Frechette GM, et al. The outcomes of Intra-Articular distal humerus open reduction and internal fixation using parallel precontoured plates in the elderly. *J Hand Surg Am*. 2023;48(8):e8301–8.
- Yu X, et al. Orthogonal plating method versus parallel plating method in the treatment of distal humerus fracture: A systematic review and meta-analysis. *Int J Surg*. 2019;69:49–60.
- Zdero R, Brzozowski P, Schemitsch EH. Biomechanical Design Optimization of Distal Humerus Fracture Plates: A Review. *Biomed Res Int*. 2024. 2024: p. 6015794.
- Yetter TR, Weatherby PJ, Somerson JS. Complications of articular distal humeral fracture fixation: a systematic review and meta-analysis. *J Shoulder Elb Surg*. 2021;30(8):1957–67.
- Tyllianakis M, et al. Long-Term functional outcomes and complications of Intra-Articular (AO type B, C) distal humerus fractures in adults: A retrospective review. *Cureus*. 2022;14(1):e21094.
- Saini R, et al. Clinical and functional outcomes of anatomical plating in distal humerus fractures in adults. *Cureus*. 2023;15(2):e35581.
- Nauth A, et al. Distal humeral fractures in adults. *J Bone Joint Surg Am*. 2011;93(7):686–700.
- Allis JB, et al. Dual versus Single-Plate fixation of midshaft clavicular fractures: A retrospective comparative study. *JB JS Open Access*. 2020;5(2):e0043. 2.
- Piggott RP, Hennessy O, Aresti NA. Distal humerus hemiarthroplasty for trauma: a systematic review of the outcomes and complications. *J Shoulder Elb Surg*. 2022;31(7):1545–52.
- Hara A, et al. Biomechanical evaluation of a transcondylar screw from the dorsolateral plate support on the stabilization of orthogonal plate configuration in distal humeral fracture. *Injury*. 2019;50(2):256–62.
- Sharma S, et al. Surgical approaches for open reduction and internal fixation of intra-articular distal humerus fractures in adults: A systematic review and meta-analysis. *Injury*. 2018;49(8):1381–91.
- Bahroun S, et al. Comparative analysis of two double-plate fixation techniques for intercondylar fractures of the distal humerus. *Sci Rep*. 2024;14(1):23913.
- Luciani AM, et al. Controversies in the management of bicolunar fractures of the distal humerus. *J Hand Surg Am*. 2023;48(2):177–86.
- Kruszewski A et al. Weak points of Double-Plate stabilization used in the treatment of distal humerus fracture through finite element analysis. *J Clin Med*. 2024; 13(4).
- Newell N, et al. Influence of testing environment and loading rate on intervertebral disc compressive mechanics: an assessment of repeatability at three different laboratories. *JOR Spine*. 2020;3(3):e21110.
- Jessup LN, et al. Validation of a musculoskeletal model for simulating muscle mechanics and energetics during diverse human hopping tasks. *R Soc Open Sci*. 2023;10(10):230393.
- Lai Y, et al. Preliminary validation of upper limb musculoskeletal model using static optimization. *Annu Int Conf IEEE Eng Med Biol Soc*. 2021;2021:4509–12.
- Kong YK et al. Ergonomic assessment of a Lower-Limb exoskeleton through electromyography and anybody modeling system. *Int J Environ Res Public Health*. 2022; 19(13).
- Peng MJ, et al. Dynamics analysis for flexion and extension of elbow joint motion based on musculoskeletal model of anybody. *Int J Med Robot*. 2021;17(6):e2321.
- Steiner M, et al. Disadvantages of interfragmentary shear on fracture healing—mechanical insights through numerical simulation. *J Orthop Res*. 2014;32(7):865–72.
- Chander DS, Cavatorta MP. Multi-directional one-handed strength assessments using anybody modeling systems. *Appl Ergon*. 2018;67:225–36.
- Giannicola G, et al. Cartilage thickness of distal humerus and its relationships with bone dimensions: magnetic resonance imaging bilateral study in healthy elbows. *J Shoulder Elb Surg*. 2017;26(5):e128–36.
- Park SH, et al. Three-dimensional osseous micro-architecture of the distal humerus: implications for internal fixation of osteoporotic fracture. *J Shoulder Elb Surg*. 2010;19(2):244–50.
- Diederichs G, et al. Three-dimensional distribution of trabecular bone density and cortical thickness in the distal humerus. *J Shoulder Elb Surg*. 2009;18(3):399–407.
- Lipphaus A, Witzel U. Finite-Element syntheses of callus and bone remodeling: Biomechanical study of fracture healing in long bones. *Anat Rec (Hoboken)*. 2018;301(12):2112–21.
- Jia Z, et al. Efficacy and safety of continuous passive motion and physical therapy in recovery from knee arthroplasty: a systematic review and meta-analysis. *J Orthop Surg Res*. 2024;19(1):68.
- O'Driscoll SW, et al. Prospective randomized trial of continuous passive motion versus physical therapy after arthroscopic release of elbow contracture. *J Bone Joint Surg Am*. 2022;104(5):430–40.
- Bolsterlee B, Veeger DH, Chadwick EK. Clinical applications of musculoskeletal modelling for the shoulder and upper limb. *Med Biol Eng Comput*. 2013;51(9):953–63.

30. Daroudi S, et al. Evaluation of ground reaction forces and centers of pressure predicted by anybody modeling system during load reaching/handling activities and effects of the prediction errors on model-estimated spinal loads. *J Biomech.* 2024;164:111974.
31. Asadi F, Arjmand N. Marker-less versus marker-based driven musculoskeletal models of the spine during static load-handling activities. *J Biomech.* 2020;112:110043.
32. Dehaghani MR, Nourani A, Arjmand N. Effects of auxetic shoe on lumbar spine kinematics and kinetics during gait and drop vertical jump by a combined in vivo and modeling investigation. *Sci Rep.* 2022;12(1):18326.
33. Mukherjee S et al. Generating human arm kinematics using reinforcement learning to train active muscle behavior in automotive research. *J Biomech Eng.* 2022; 144(12).
34. Charles JP, Cappellari O, Hutchinson JR. A dynamic simulation of musculoskeletal function in the mouse hindlimb during trotting locomotion. *Front Bioeng Biotechnol.* 2018;6:61.
35. Dubowsky SR, et al. Validation of a musculoskeletal model of wheelchair propulsion and its application to minimizing shoulder joint forces. *J Biomech.* 2008;41(14):2981–8.

Publisher's note

Springer Nature remains neutral with regard to jurisdictional claims in published maps and institutional affiliations.